Supporting Information

Multi-functional modification of nickel-rich lithium cathode materials using Na_2PO_3F

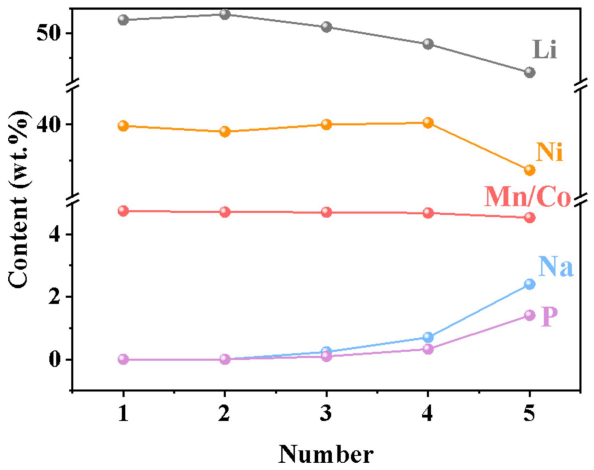

Fig.S1 Components of NCM sample. ICP-OES of samples before cycle and 1, 2, 3, 4 and 5 corresponding to NCM-0, NCM-0.05, NCM-0.33, NCM-1 and NCM-3, respectively.

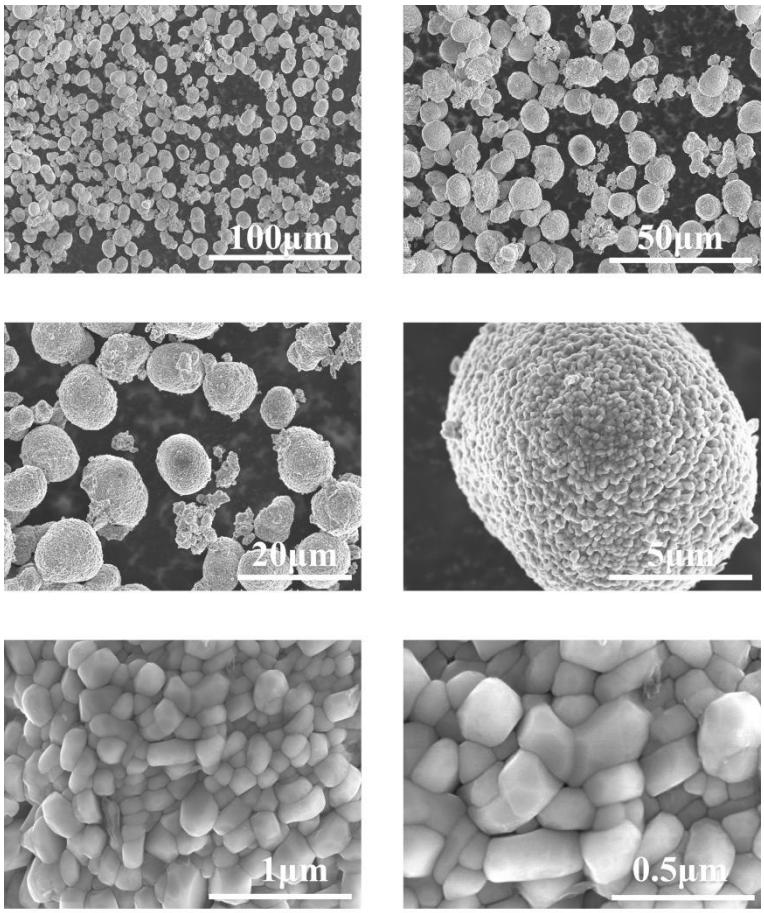

Fig.S2 Morphology characterizations of NCM-0. SEM image of NCM-0 in different magnification and corresponding to 500 ×, 1 k×, 2 k×, 10 k×, 50 k×, 100 k×, respectively.

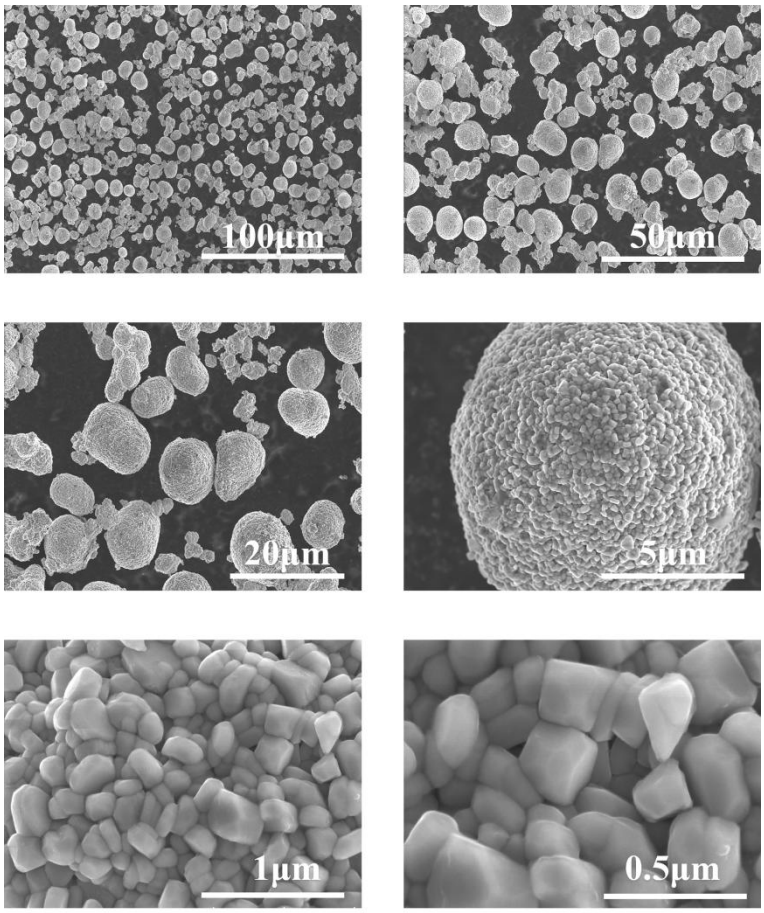

Fig.S3 Morphology characterizations of NCM-0.05. SEM image of NCM-0.05 in different magnification and corresponding to 500 ×, 1 k×, 2 k×, 10 k×, 50 k×, 100 k×, respectively.

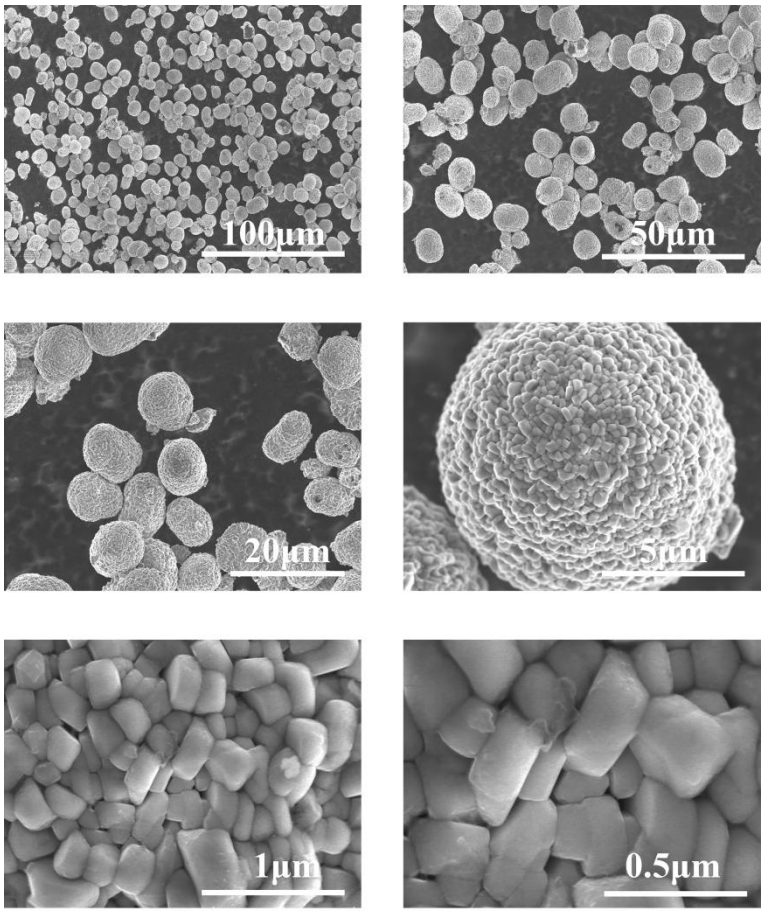

Fig.S4 Morphology characterizations of NCM-0.33. SEM image of NCM-0.33 in different magnification and corresponding to 500 ×, 1 k×, 2 k×, 10 k×, 50 k×, 100 k×, respectively.

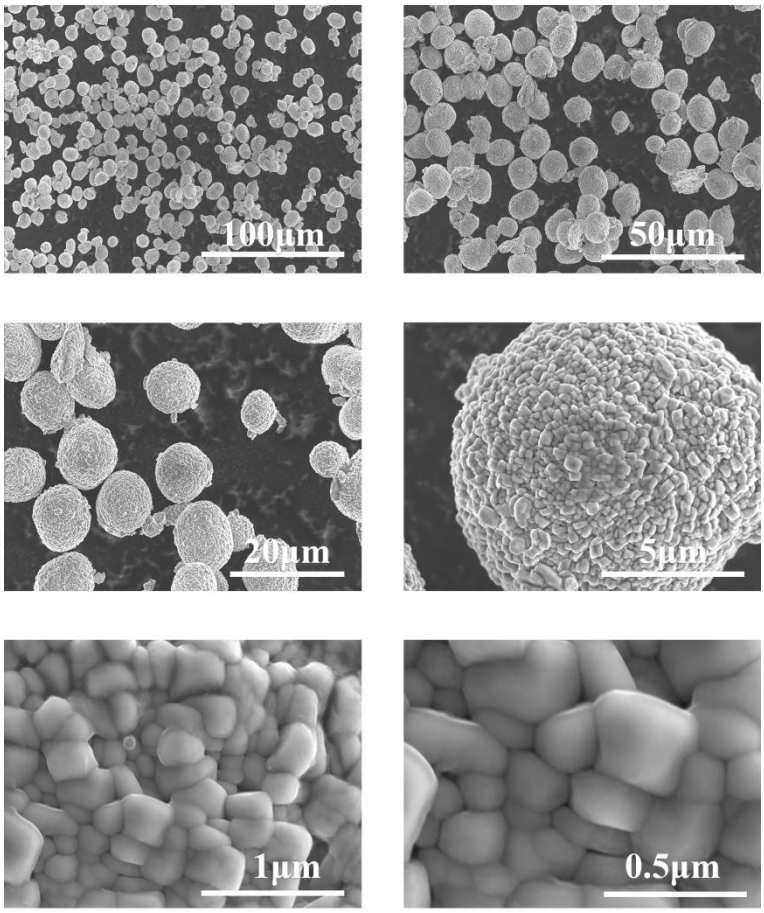

Fig.S5 Morphology characterizations of NCM-1. SEM image of NCM-1 in different magnification and corresponding to 500 ×, 1 k×, 2 k×, 10 k×, 50 k×, 100 k×, respectively.

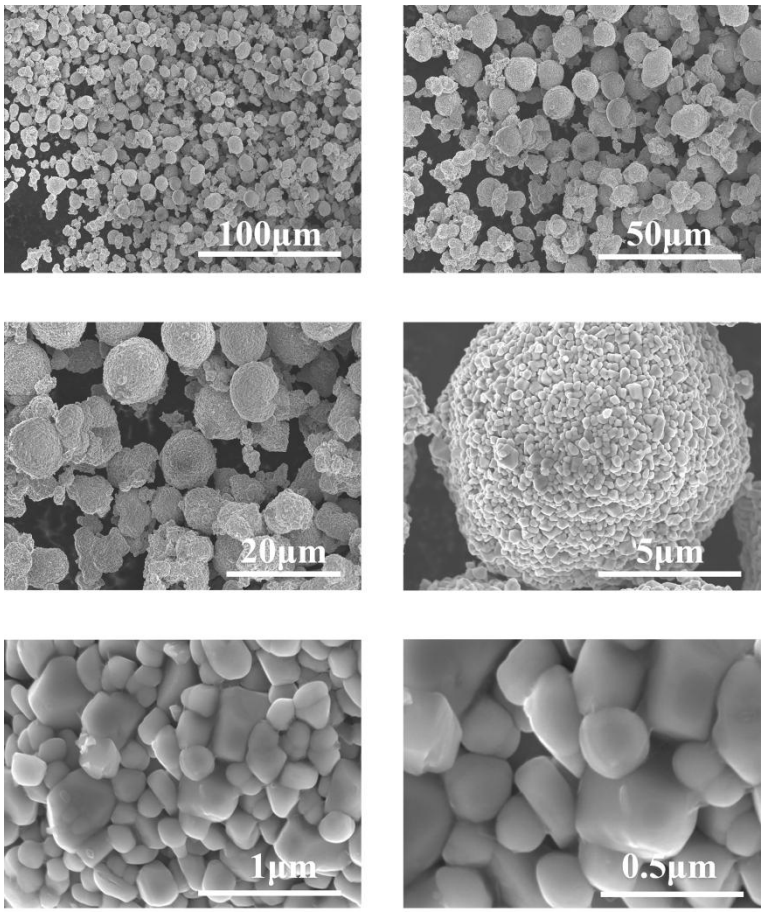

Fig.S6 Morphology characterizations of NCM-3. SEM image of NCM-3 in different magnification and corresponding to 500 ×, 1 k×, 2 k×, 10 k×, 50 k×, 100 k×, respectively.

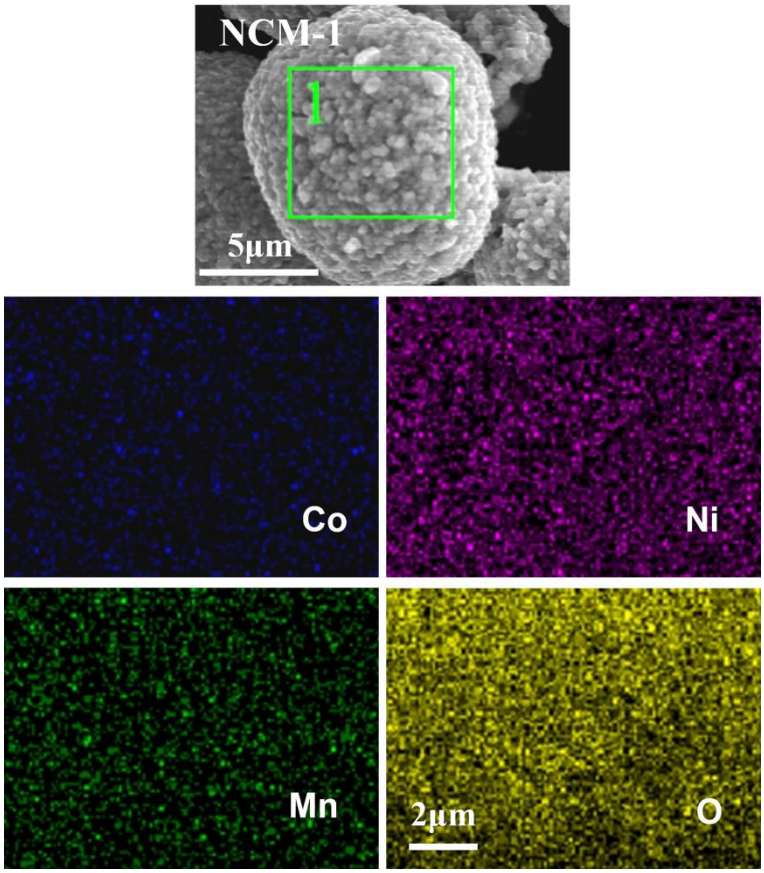

Fig.S7 Morphology characterizations of NCM-1. EDS mapping of NCM-1 and the Co, Ni, Mn and O elements were evenly distributed.

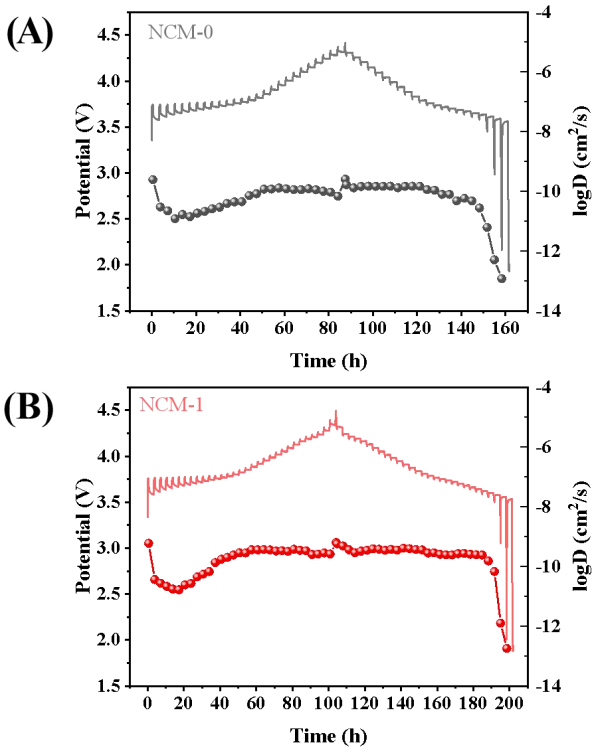

Fig.S8 Electrochemical Performance characterizations. Charge/discharge curves of GITT at initial cycle for (A) NCM-0 and (B) NCM-1 in the range of 2.8-4.4 V (vs. Li^+/Li) at 25 ℃. GITT measurements were conducted in a titration step at 0.08 C of 30 min and a relaxation step of 3 h.

The D_{Li^+} can be calculated by the Fick's second law through Equation (1):[1]

$$D_{Li^+} = \frac{4}{\pi\tau}\left(\frac{m_B V_M}{M_B S}\right)^2\left(\frac{\Delta E_s}{\Delta E_t}\right)^2 \quad (1)$$

Where the τ is the relaxation time (τ = 1800 s), m_B is the weight of the active material of electrode material, V_M is the molar volume of electrode material, M_B is the molar mass of the active material of electrode material (M_B = 97.5 g mol^{-1}), S is the contact area of electrode material with electrolyte (S = 1.131 cm^2), ΔE_s is the voltage change caused by the pulse, and ΔE_t is the constant current charge/discharge voltage change.

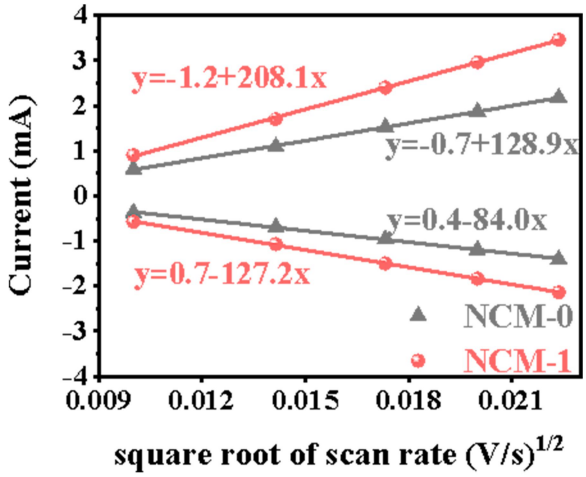

Fig.S9 CV curves of NCM-0 and NCM-1. The lines plot of cathodic/anodic peak current densities with the square root of scan rate.

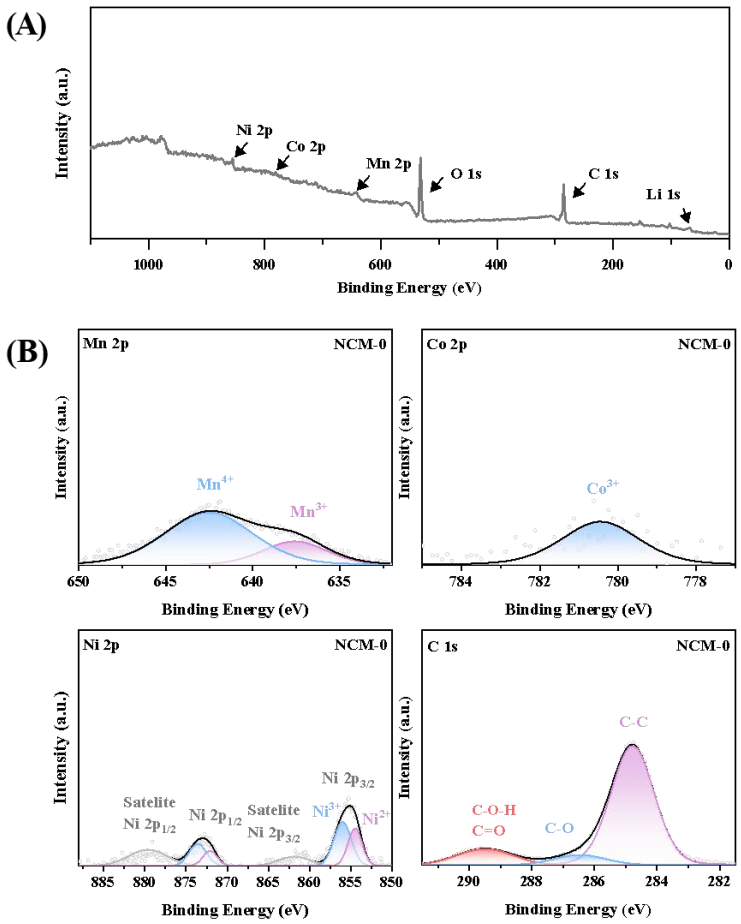

Fig.S10 Surface composition characterization of NCM-0. (A) XPS full spectrum of NCM-0. (B) XPS spectra of Mn 2p, Co 2p, Ni 2p and C 1s for NCM-0.

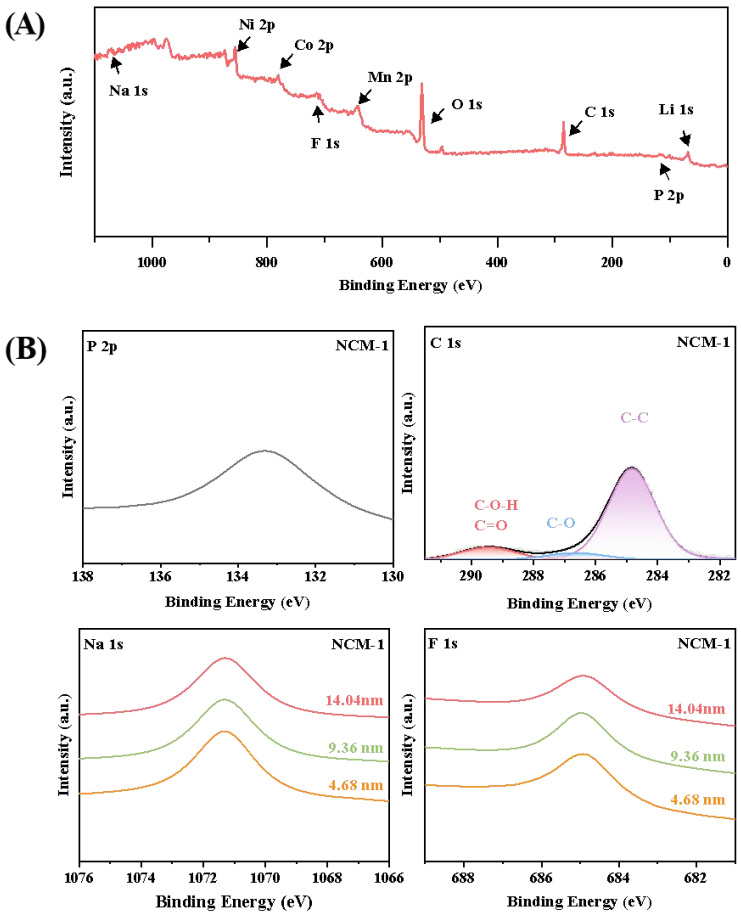

Fig.S11 Surface composition characterization of NCM-1. (A) XPS full spectrum of NCM-1. (B) XPS spectra of P 2p and C 1s for NCM-1, also the deep profile curve of Na and F in the surface of NCM-1. The binding energy of 1070-1072 eV were corresponding to Na-O and Na-F,and the binding energy of 684-686 eV were corresponding to Li-F, TM-F and Na-F, with the binding energy of 132-135 eV were corresponding to Li-O-P.

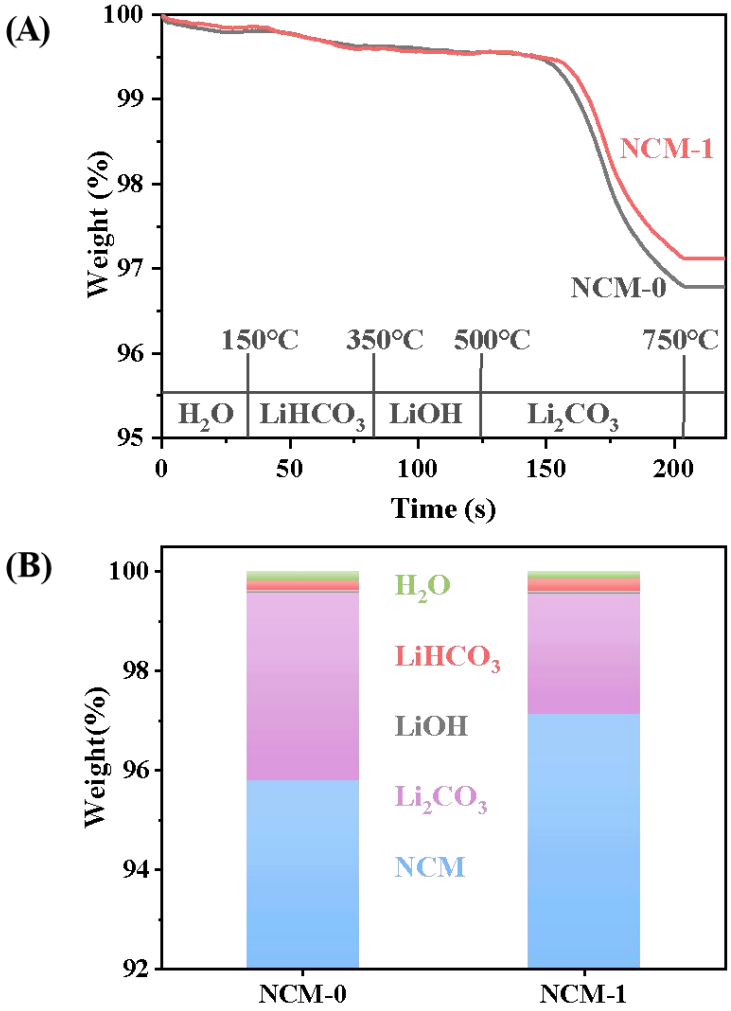

Fig.S12 Surface composition of NCM-1 and NCM-1. (A) TGA test and (B) the content of the material decomposition during each pyrolysis process: (i) Adsorbed water should be highly unsTable Sat 150 ℃ and is expected to evaporate from the sample relatively quickly. (ii) Lithium bicarbonate and adsorbed carbonate species on positive electrode materials will decompose at 350 ℃. (iii) LiOH is thermally degraded at 410-450 ℃ and Li_2CO_3 is evolved at 710-750 ℃.[2]

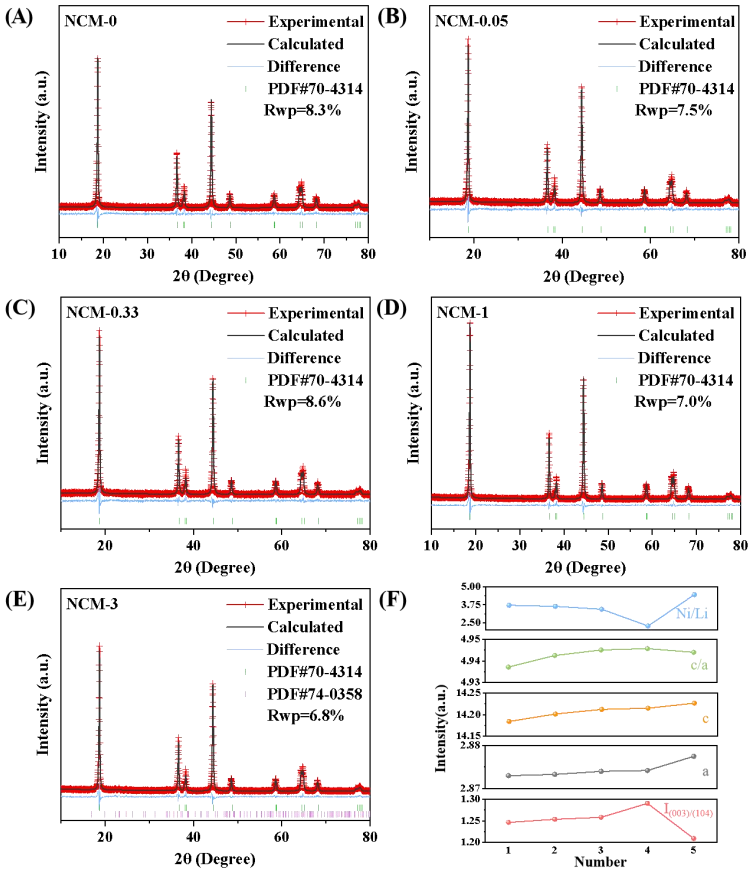

Fig.S13 Structural characterization of five sample. XRD patterns of (A) NCM-0, (B) NCM-0.05, (C) NCM-0.33, (D) NCM-1 and (E) NCM-3 with refined XRD data analysis. (F) The lattice parameters of all samples.

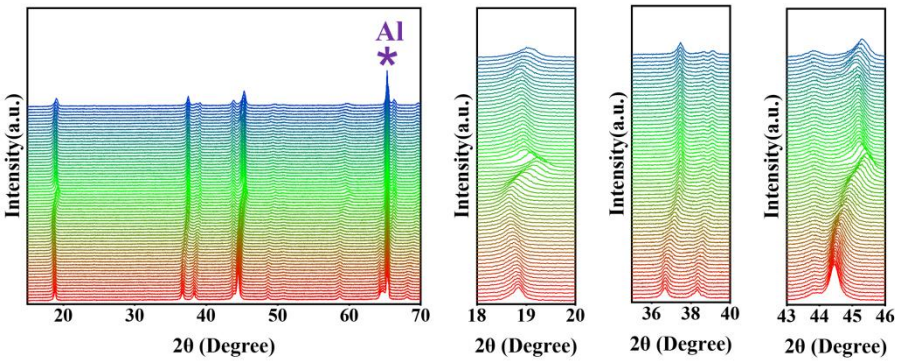

Fig.S14 Structural evolution of NCM-0. In-situ XRD for NCM-0 cathode during the first charge-discharge cycle between 2.8-4.4 V (vs. Li^+/Li) at 0.08 C. The peak corresponding to the * was the signal of the basal Al.

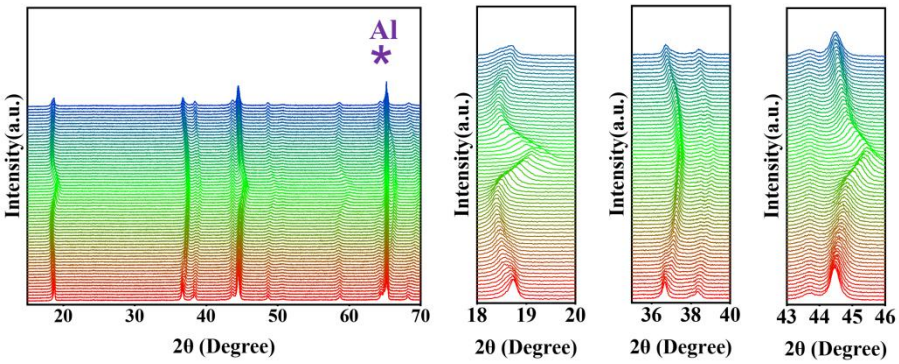

Fig.S15 Structural evolution of NCM-1. In-situ XRD for NCM-1 cathodes during the first charge/discharge cycle between 2.8-4.4 V (vs. Li^+/Li) at 0.08 C. The peak corresponding to the * was the signal of the basal Al.

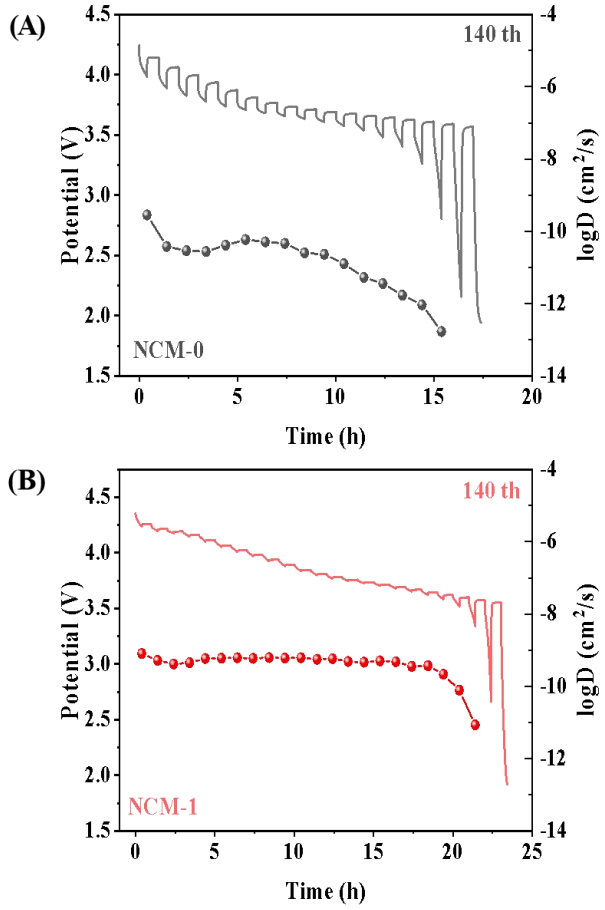

Fig.S16 Electrochemical Performance characterizations. Charge/discharge curves of GITT at 140th cycle for (A) NCM-0 and (B) NCM-1 in the range of 2.8-4.4 V (vs. Li^+/Li) at 25 ℃.

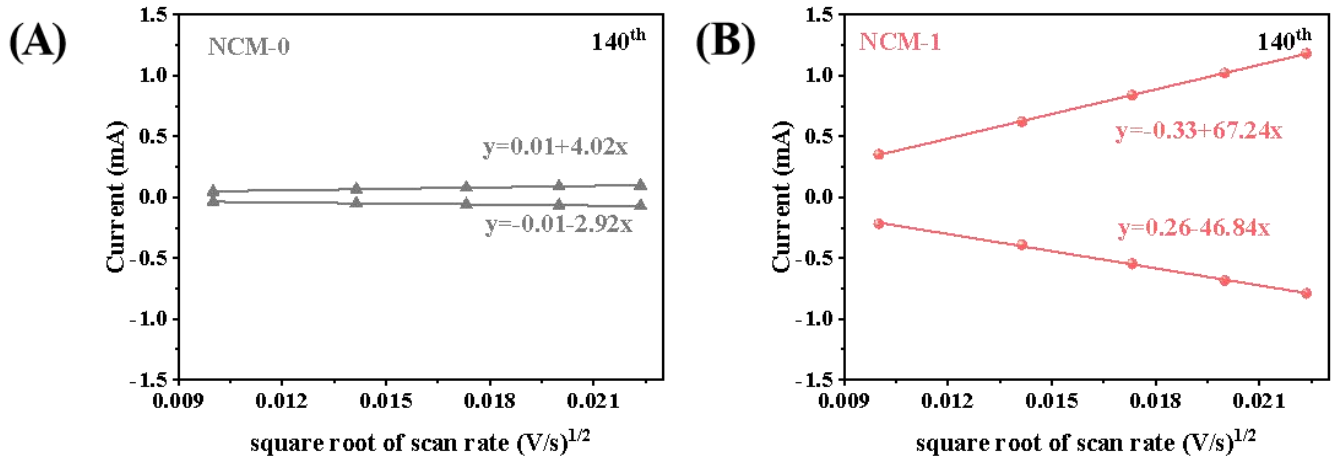

Fig.S17 Lines plot of cathodic/anodic peak current densities with the square root of scan rate of (A) NCM-0 and (B) NCM-1 at the 140th.

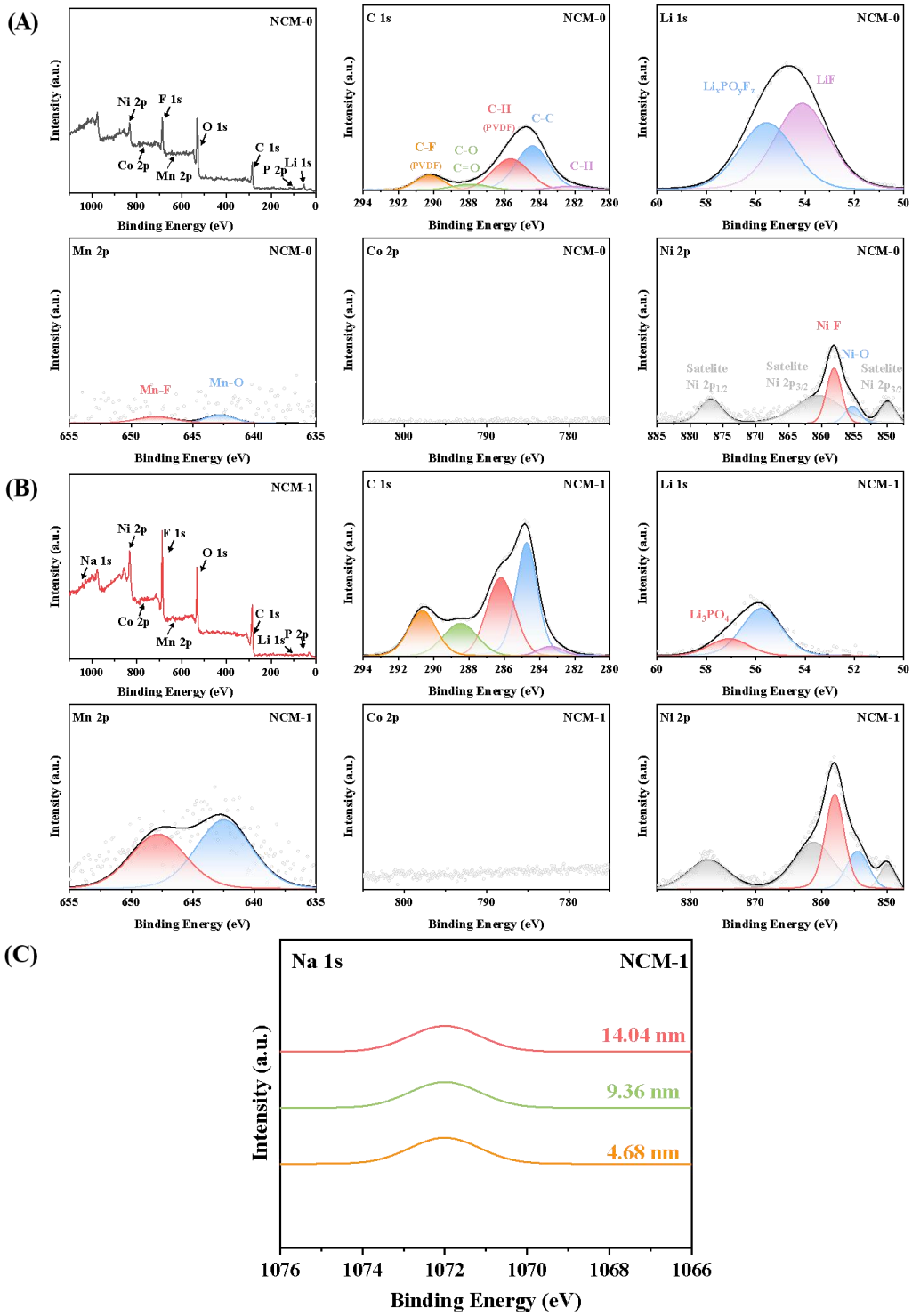

Fig.S18 Surface composition characterization. XPS spectra of Su 1s, C 1s, Li 1s, Mn 2p, Co 2p and Ni 2p of (A) NCM-0 and (B) NCM-1 at the 140th. (C) The deep profile curve of Na for NCM-1.

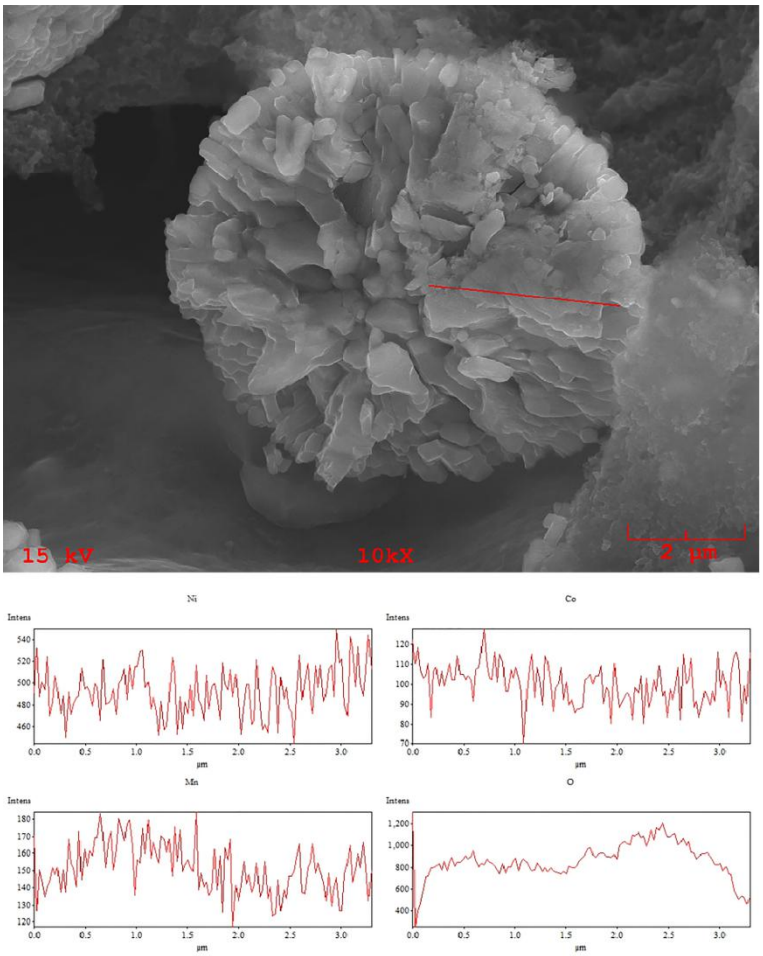

Fig.S19 Structural characterization of NCM-0. Cross-sectional SEM images of NCM-0 at the 280th and the content of the O, Mn, Co and Ni elements distribute along the bulk to the surface.

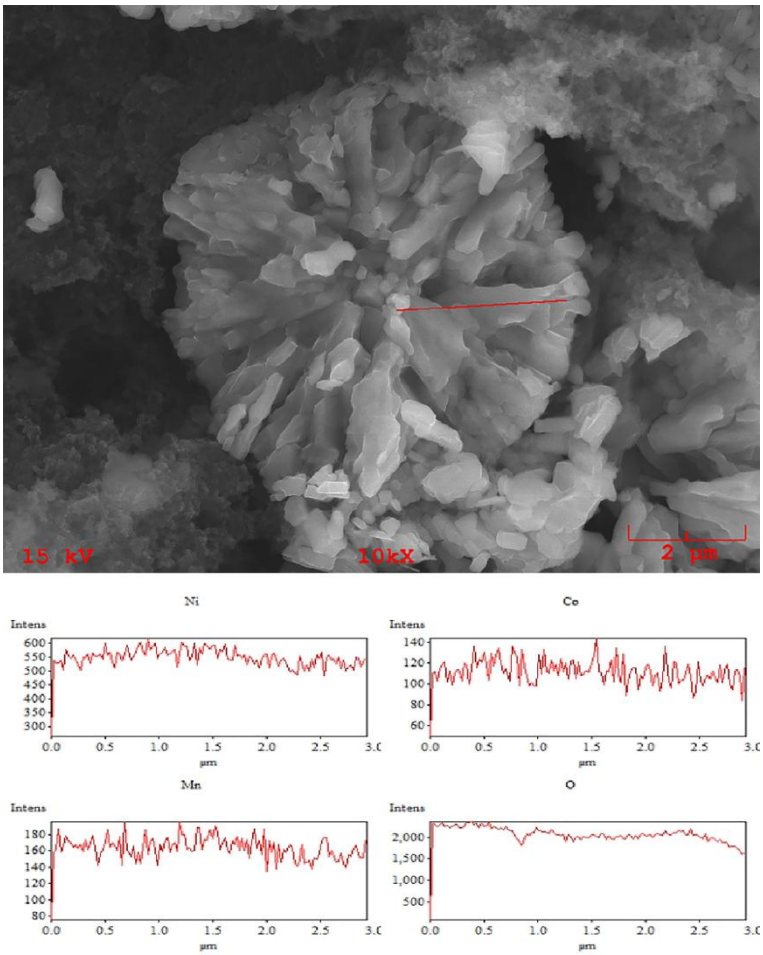

Fig.S20 Structural characterization of NCM-1. Cross-sectional SEM images of NCM-1 at the 280th and the content of the O, Mn, Co and Ni elements distribute along the bulk to the surface.

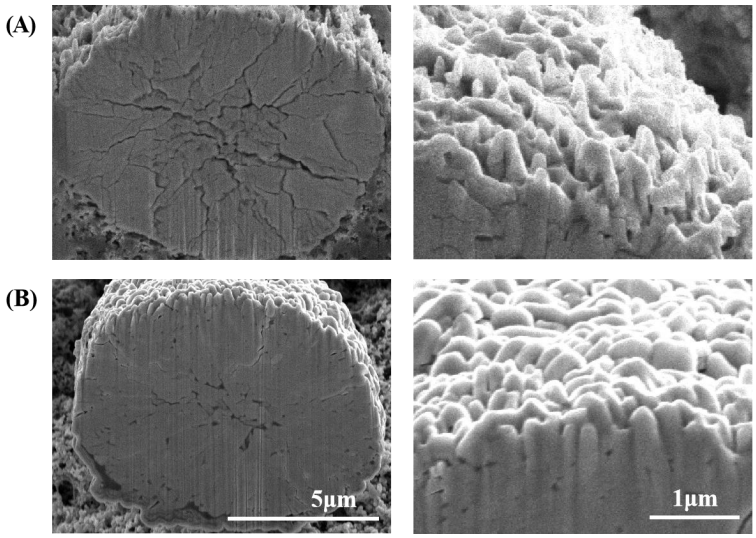

Fig.S21 Structural characterization. Cross-sectional SEM images of (A) NCM-0 and (B) NCM-1 at the 280th and the corresponding the morphology of the particle surface (samples were prepared through a focused ion beam).

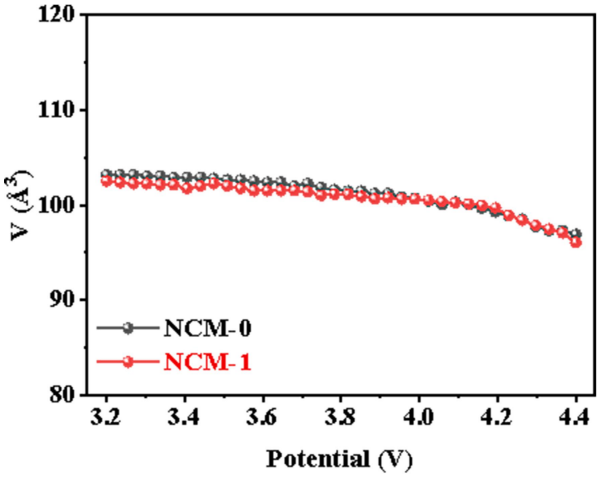

Fig.S22 The change of cell volume V of NCM-0 and NCM-1 cathodes during the first charge between 2.8-4.4 V (vs. Li^+/Li) at 25 ℃.

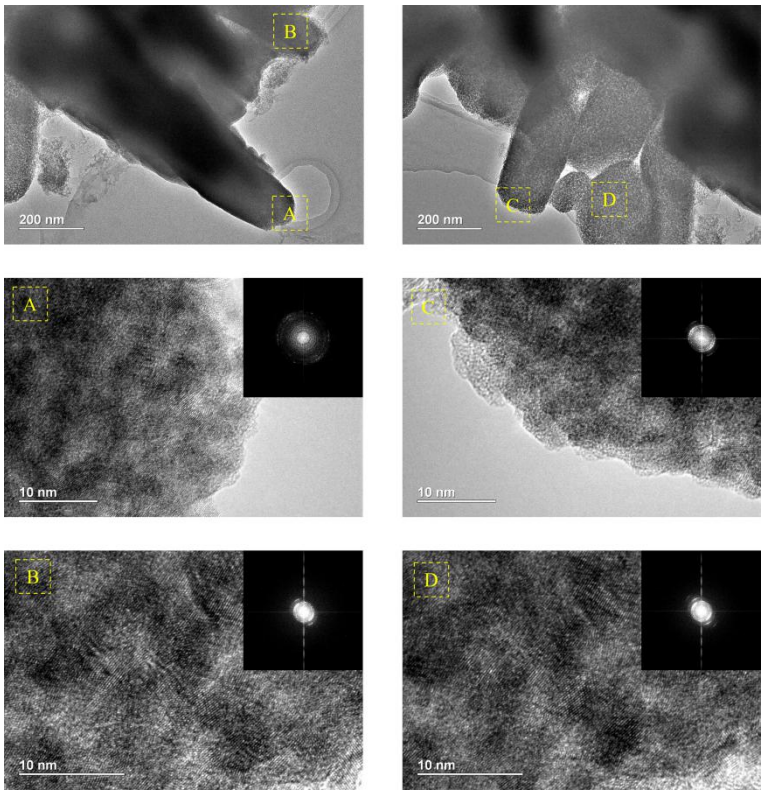

Fig.S23 Structural characterization. TEM images of NCM-0 at the 140th with the magnification of the A, B, C and D region and the corresponding FFT pattern (inset).

Supporting Tables

Table S1 Comparison of cycle number and capacity retention for reported modification of layer oxide cathode materials[3-8] and this work.

	C-Rate (C)	Voltage (V)	Capacity retention (%)	Electrolyte	Reference
NCM811-Na_2PO_3F	1	4.4	100.0 (at 50 cycles) 99.3 (at 100 cycles) 94.4 (at 200 cycles) 90.0 (at 300 cycles) 83.3 (at 400 cycles)	0.8 M $LiPF_6$ 0.4 M LiDFOB EC/EMC/FEC	This work
NCM811-$Li_n(TM)_mPO_4$	1	4.5	80.4 (at 300 cycles) 87.0 (at 200 cycles)	1 M $LiPF_6$ EC/DEC/DMC	[3]
NCM811-Li_3PO_4	1	4.3	86.7 (at 200 cycles)	1 M $LiPF_6$ EC/EMC/DMC	[4]
NCM811-$LaPO_4$	1	4.3	91.2 (at 100 cycles)	-	[5]
NCM811-F	2	4.3	94.3 (at 100 cycles)	1 M $LiPF_6$ EC/EMC/DMC	[6]
NCM532-Na	-	4.25	97.8 (at 50 cycles)	1 M $LiPF_6$ EC/DMC	[7]
LNM120206-F Na&F	1	4.8	82.0 (at 100 cycles)	1 M $LiPF_6$ EC/DMC	[8]
LNM120206-Na	1	4.8	91.0 (at 100 cycles)	1 M $LiPF_6$ EC/DMC	[8]
LNM120206-Na&F	1	4.8	93.0 (at 100 cycles)	1 M $LiPF_6$ EC/DMC	[8]

Table S2 The R_e and R_{sf} of the NCM-0 and NCM-1 measured by EIS.

Number	R_e (Ω)	R_{sf} (Ω)	σ
NCM-0	36.04	112.80	6.77
NCM-1	23.87	59.81	35.93

The EIS results is commonly divide into three regions: (i) a intercept in the high frequency region relates to the electrolyte resistance (R_e); (ii) a semicircle in the high frequency region represents to the the surface-film resistance (R_{sf}); (iii) a semicircle in the intermediate frequency region relates to the charge transfer impedance (R_{ct}) of the Li-ion/electron at the interface between the electrolyte and the positive electrode material; (iiii) a sloping line in the low frequency region corresponds to the Warburg impedance relates to the diffusion movement of Li-ions inside the positive electrode material.[9, 10]

Table S3 The oxidation and reduction peak current of the NCM-0 and NCN-1 with a scan rate of 0.1-0.5 mV s^{-1}, and corresponding lithium-ion diffusion coefficient.

Number	NCM-0 Oxidation	NCM-0 Reduction	NCM-1 Oxidation	NCM-1 Reduction
I_p at 0.1mVs^{-1}	0.60	-0.37	0.90	-0.58
I_p at 0.2mVs^{-1}	1.09	-0.69	1.70	-1.07
I_p at 0.3mVs^{-1}	1.53	-0.96	2.40	-1.50
I_p at 0.4mVs^{-1}	1.87	-1.20	2.96	-1.84
I_p at 0.5mVs^{-1}	2.18	-1.41	3.46	-2.14
$I_p/v^{1/2}$	128.91	-83.96	208.11	-127.17
D_{Li}^+	6.92E-10	2.94E-10	1.80E-09	6.74E-10

CV observed the behavior of the D_{Li}^+(cm^2 s^{-1}) during the different scan rates.[9] According to the plot of CV scan rates $v^{1/2}$ (mV s^{-1})$^{1/2}$ versus the peak current I_p (mA), D_{Li}^+ of samples are estimated as below (2):[11]

$$I_p = 2.69 \times 10^5 \times n^{3/2} \times A \times {D_{Li^+}}^{1/2} \times v^{1/2} \times C_0 \quad (2)$$

Where n is the number of electrons in the Li^+ (n = 1), A is the electrode area (A = 1.131 cm^2), and C_0 is the initial concentration of Li^+ in the cathode (C_0 = 0.018 mol cm^{-3}).

Table S4 The relative composition of Li and TM (Ni/Mn/Co) in the NCM-0 and NCM-1.

Number	Li	TM	Li/TM
NCM-0	10.650	10.392	1.025
NCM-1	10.581	10.482	1.009

Table S5 Crystallographic and refined XRD data of NCM-0, NCM-0.05, NCM-0.33, NCM-1 and NCM-3.

Number	NCM-0	NCM-0.05	NCM-0.33	NCM-1	NCM-3
***a*[Å]**	2.873	2.873	2.874	2.874	2.878
***c*[Å]**	14.184	14.201	14.212	14.215	14.227
c/a	4.937	4.946	4.945	4.946	4.944
V[Å^3]	101.386	101.534	101.659	101.692	102.014
$I_{(003)/(104)}$	1.246	1.256	1.258	1.291	1.209
Ni at Li site (%)	3.72	3.64	3.44	2.27	4.46
R_{wp} **(%)**	8.3	7.5	8.6	7	6.8

Table S6 Refined XRD data for NCM-0.

Element	Site	x	y	z	Occupancy
Li	(3*a*)	0	0	0	0.963
Ni	(3*a*)	0	0	0	0.037
Ni	(3*b*)	0	0	0.5	0.763
Co	(3*b*)	0	0	0.5	0.100
Mn	(3*b*)	0	0	0.5	0.100
Li	(3*b*)	0	0	0.5	0.037
O	(6*c*)	0	0	0.242	2.000

Table S7 Refined XRD data for NCM-0.05 (Since the content of Na_2PO_3F was too small, the effect of Na and F elements on the crystal structure of the NCM was ignored during the refined).

Element	Site	x	y	z	Occupancy
Li	(3*a*)	0	0	0	0.964
Ni	(3*a*)	0	0	0	0.036
Na	(3*a*)	0	0	0	<0.001
Ni	(3*b*)	0	0	0.5	0.764
Co	(3*b*)	0	0	0.5	0.100
Mn	(3*b*)	0	0	0.5	0.100
Li	(3*b*)	0	0	0.5	0.036
O	(6*c*)	0	0	0.243	2.000
F	(6*c*)	0	0	0.243	<0.001

Table S8 Refined XRD data for NCM-0.33.

Element	Site	x	y	z	Occupancy
Li	(3*a*)	0	0	0	0.957
Ni	(3*a*)	0	0	0	0.034
Na	(3*a*)	0	0	0	0.009
Ni	(3*b*)	0	0	0.5	0.766
Co	(3*b*)	0	0	0.5	0.100
Mn	(3*b*)	0	0	0.5	0.100
Li	(3*b*)	0	0	0.5	0.034
O	(6*c*)	0	0	0.242	1.996
F	(6*c*)	0	0	0.242	0.004

Table S9 Refined XRD data for NCM-1.

Element	Site	x	y	z	Occupancy
Li	(3*a*)	0	0	0	0.964
Ni	(3*a*)	0	0	0	0.023
Na	(3*a*)	0	0	0	0.013
Ni	(3*b*)	0	0	0.5	0.777
Co	(3*b*)	0	0	0.5	0.100
Mn	(3*b*)	0	0	0.5	0.100
Li	(3*b*)	0	0	0.5	0.023
O	(6*c*)	0	0	0.240	1.992
F	(6*c*)	0	0	0.240	0.008

Table S10 Refined XRD data for NCM-3.

Element	Site	x	y	z	Occupancy
Li	(3*a*)	0	0	0	0.920
Ni	(3*a*)	0	0	0	0.045
Na	(3*a*)	0	0	0	0.035
Ni	(3*b*)	0	0	0.5	0.755
Co	(3*b*)	0	0	0.5	0.100
Mn	(3*b*)	0	0	0.5	0.100
Li	(3*b*)	0	0	0.5	0.045
O	(6*c*)	0	0	0.240	1.980
F	(6*c*)	0	0	0.240	0.020

Table S11 The oxidation and reduction peak current of the NCM-0 and NCN-1 with a scan rate of 0.1-0.5 mV s^{-1}, and corresponding lithium-ion diffusion coefficient after 140th cycle.

Number	NCM-0 Oxidation	NCM-0 Reduction	NCM-1 Oxidation	NCM-1 Reduction
I_p at 0.1mVs^{-1}	0.05	-0.04	0.35	-0.22
I_p at 0.2mVs^{-1}	0.07	-0.05	0.62	-0.39
I_p at 0.3mVs^{-1}	0.08	-0.06	0.84	-0.55
I_p at 0.4mVs^{-1}	0.09	-0.07	1.02	-0.68
I_p at 0.5mVs^{-1}	0.10	-0.07	1.18	-0.79
$I_p/v^{1/2}$	4.02	2.92	67.24	46.84
D_{Li}^+	6.73E-13	3.55E-13	1.88E-10	9.14E-11

References

1 S. Cui, Y. Wei, T. Liu, W. Deng, Z. Hu, Y. Su, H. Li, M. Li, H. Guo, Y. Duan, W. Wang, M. Rao, J. Zheng, X. Wang and F. Pan, *Adv. Energy Mater.*, 2016, **6**, 1501309-1501318.

2 H. Liu, Y. Yang and J. Zhang, *J. Power Sources*, 2006, **162**, 644-650.

3 Y. Li, L. Cui, C. Tan, X. Fan, Q. Pan, Y. Chu, S. Hu, F. Zheng, H. Wang and Q. Li, *Chem. Eng. J.*, 2022, **430**, 132985-132996.

4 P. Yue, Z. Wang, H. Guo, X. Xiong and X. Li, *Electrochim. Acta*, 2013, **92**, 1-8.

5 W. Zhang, L. Liang, F. Zhao, Y. Liu, L. Hou and C. Yuan, *Electrochim. Acta*, 2020, **340**, 135871-135881.

6 H. Tong, P. Dong, J. Zhang, J. Zheng, W. Yu, K. Wei, B. Zhang, Z. Liu and D. Chu, *J. Alloys Compd.*, 2018, **764**, 44-50.

7 R. Zhao, Z. Yang, J. Liang, D. Lu, C. Liang, X. Guan, A. Gao and H. Chen, *J. Alloys Compd.*, 2016, **689**, 318-325.

8 D. Liu, X. Fan, Z. Li, T. Liu, M. Sun, C. Qian, M. Ling, Y. Liu and C. Liang, *Nano Energy*, 2019, **58**, 786-796.

9 K. Du, H. Xie, G. Hu, Z. Peng, Y. Cao and F. Yu, *ACS Appl. Mater. Interfaces*, 2016, **8**, 17713-17720.

10 J. Zhang, Y. Cao, X. Ou, J. Zhang, C. Wang, C. Peng, B. Zhang and Y. Tian, *J. Power Sources*, 2019, **436**, 226722-226731.

11 W. Liu, X. Li, D. Xiong, Y. Hao, J. Li, H. Kou, B. Yan, D. Li, S. Lu, A. Koo, K. Adair and X. Sun, *Nano Energy*, 2018, **44**, 111-120.

